

A Gravitational Wave Background from Intermediate Mass Black Holes in AGN Disks

Chiara M. F. Mingarelli

Department of Physics, Yale University, New Haven, CT 06520, USA^{*}

(Dated: February 11, 2026)

Intermediate mass black holes (IMBHs) formed in active galactic nucleus (AGN) disks are expected to inspiral into their central supermassive black holes (SMBHs), generating a stochastic gravitational-wave (GW) background in the mHz–decihertz band. Using the population-agnostic energetic formalism, we treat the AGN-disk channel as a mass-flow pipeline connecting the stellar-mass black hole population observed by LIGO/Virgo/KAGRA (LVK) to the SMBH mass reservoir via IMBHs. By anchoring this estimate to the LVK merger rate densities and the cosmic SMBH mass density derived from scaling relations, we derive a limit on the background amplitude. We show that the total energy density of the background is bounded by the global mass budget of SMBH growth. For fiducial parameters consistent with the fourth Gravitational-Wave Transient Catalog (GWTC-4), this yields a characteristic strain $A_{\text{IMR}} \simeq (1.2^{+0.2}_{-0.2}) \times 10^{-21}$ at 3 mHz. While this fiducial amplitude is subdominant to the Galactic white dwarf foreground and the stellar-mass Extreme Mass Ratio Inspiral (EMRI) background, we show it can be distinguished by its non-Gaussian statistics and higher frequency cutoff. This new background may be detectable in the decihertz band where proposed detectors such as the Big Bang Observer or long-baseline lunar interferometers can measure it cleanly. A detection would provide a direct, model-independent constraint on the efficiency with which AGN disks process stellar remnants into SMBH mass growth, linking the LVK and LISA bands.

I. INTRODUCTION

The detection of gravitational waves (GWs) from the mergers of stellar-mass binary black holes (BBHs) has reshaped black hole astrophysics across the mass scale [1]. Ground-based detectors have now cataloged a large population of BBH mergers in the tens-to-thousands of hertz band, revealing massive stellar remnants and merger products that likely include second-generation black holes [2]. A leading formation channel for the most massive systems, including events such as GW190521 [3], is hierarchical growth in the accretion disks of active galactic nuclei (AGN) [4]. In these dense, gas-rich environments, black holes can migrate, accrete, and merge repeatedly, plausibly building intermediate-mass black holes (IMBHs) in the 10^2 – $10^4 M_\odot$ range.

At the opposite end of the mass spectrum, pulsar timing arrays (PTAs) are converging on evidence for a nanohertz stochastic background consistent with the inspiral of supermassive black hole binaries (SMBHBs) with masses 10^8 – $10^{10} M_\odot$ (see, e.g., Sesana and Figueroa [5]). Between these observational windows lies the milli- to-decihertz band (10^{-4} – 10^{-1} Hz), which will be probed by the Laser Interferometer Space Antenna (LISA) [6] and proposed follow-on missions such as BBO [7]. This band is where intermediate-mass-ratio inspirals (IMRIs) and extreme mass-ratio inspirals (EMRIs) are expected to contribute a rich GW landscape, and where different channels for building and feeding SMBHs can be tested.

If AGN disks efficiently produce IMBHs, then a generic outcome is that some fraction of those IMBHs will ultimately be delivered to the central SMBH, producing

IMBH–SMBH inspirals. The superposition of this population across cosmic time generates a gravitational-wave background (GWB) in the mHz–decihertz band, which we call the AGN–IMRI GWB. This signal is distinct from the PTA background and the LISA white dwarf foreground. It encodes the time-integrated efficiency with which AGN disks and related nuclear environments process compact objects into SMBH mass growth.

This work applies the general energetic formalism derived in the companion paper, Mingarelli 2026a [8], to the specific case of the AGN–IMRI background. First, we derive an empirically anchored benchmark for the AGN–IMRI background amplitude and spectrum, using a deliberately conservative, bottom-up construction that does not require detailed modeling of AGN disk micro-physics. Second, we place this background in context: we compare it to other expected stochastic components in the LISA and decihertz bands, especially the EMRI background, and we assess whether these extragalactic components can be separated from the dominant Galactic foreground from double white dwarfs (DWDs).

Our approach is a mass-flow and mass-budget argument. We treat the AGN-disk channel as a pipeline linking two robust observables: (i) the LVK merger rate density that constrains how much stellar-remnant mass is being processed through compact-object mergers today [1], and (ii) the local SMBH mass density inferred from galaxy scaling relations, which sets the total cosmological mass reservoir available for SMBH assembly. This second ingredient is the key global constraint: regardless of how IMBHs form, the total mass delivered through IMBH captures cannot exceed the SMBH mass budget. Within this framework we derive a closed-form normalization for an inspiral-like background and identify a hard astrophysical ceiling set by SMBH demographics [9, 10].

A central complication is that in the mHz band the

^{*} chiara.mingarelli@yale.edu

Galactic DWD foreground dominates the strain power and shares an inspiral-like spectral slope [11]. Spectral shape alone is therefore not a reliable discriminator. Furthermore, a background from stellar-mass EMRIs may also exist in this band. We show that the Galactic foreground can be removed via annual modulation analysis, while the stellar-EMRI background can be distinguished from the AGN-IMRI signal via statistical properties: the former is a Gaussian confusion noise, while the latter is a non-Gaussian popcorn signal due to the rarity of massive IMBH events.

The paper is organized as follows. In Sec. II we define the AGN-IMRI capture channel and its connection to AGN-assisted growth. In Sec. III we derive the background normalization from energy conservation, and in Sec. IV we present the resulting spectrum and amplitude range, including a conservative benchmark and a saturation ceiling. In Sec. V we compare this channel to other proposed AGN-IMRI formation pathways and clarify terminology in the IMRI literature. In Sec. VI we discuss component separation, including removing the DWD foreground and distinguishing AGN-IMRIs from stellar EMRIs. In Sec. VII we place the signal in the broader mHz-decibertz landscape by comparing to other astrophysical GWBs and dominant foregrounds. We discuss interpretation, discriminants, and key uncertainties in Sec. VIII, and conclude in Sec. IX.

II. THE AGN-IMRI CAPTURE CHANNEL

We derive a GWB for AGN-IMRI captures by treating the AGN-disk channel as a mass-flow pipeline that connects LVK- and LISA-band sources. In this picture, stellar-mass black holes, constrained by LVK merger rates, undergo hierarchical mergers and gas accretion in AGN disks to form IMBHs [12, 13]. These IMBHs then inspiral into the central SMBH, producing a background of IMRIs in the millihertz to decibertz band. This construction links the stellar-mass reservoir to the supermassive reservoir: a LISA or decibertz-band detection would directly probe the efficiency with which AGN disks process LVK-band remnants into SMBH mass growth.

Unlike forward models that assume an arbitrary efficiency for hierarchical growth, we anchor this estimate to merger rate densities inferred from current ground-based observations. This bottom-up approach assumes that the IMBH population indicated by LVK events (e.g., GW190521 [3]) represents a cosmological population that, if produced in AGN disks, will ultimately either (i) be retained and delivered to the central SMBH, or (ii) be depleted through alternate fates (ejection, disk exit, or mergers not followed by capture). We encapsulate these possibilities in a single mass fraction parameter, f_{IMR} , defined as the fraction of the present-day SMBH mass density accumulated through the capture of IMBHs:

$$f_{\text{IMR}} \equiv \frac{\rho_{\text{IMR}}}{\rho_{\bullet}}, \quad (1)$$

where ρ_{IMR} is the comoving mass density in IMBHs that inspiral into SMBHs through this channel and ρ_{\bullet} is the total local SMBH mass density.

III. THE AGN-IMRI BACKGROUND

The total BBH merger rate observed by LVK is $R_{\text{BBH}}^{\text{obs}} \sim 14\text{--}26 \text{ Gpc}^{-3} \text{ yr}^{-1}$ [1]. Only a fraction f_{AGN} of these mergers occur in AGN disks, where hierarchical growth can build IMBHs. Comparing the resulting IMBH mass density to the total SMBH mass density $\rho_{\bullet} = (1.8_{-0.5}^{+0.8}) \times 10^6 M_{\odot} \text{ Mpc}^{-3}$ [14] implies a small fiducial mass fraction f_{IMR} (evaluated in Sec. IV), significantly more conservative than theoretical upper limits which assume high efficiency in the sequential hierarchical growth, $f_{\text{IMR}} \propto f_{\text{AGN}} f_{\text{trap}} g_{\text{grow}}$, where f_{AGN} is the fraction of BBHs in AGN disks and g_{grow} parameterizes gas-driven growth [4, 15, 16]. While theoretical models allowing for efficient trapping and runaway growth can yield f_{IMR} as high as 0.05 (5%) [4], we restrict our prediction to the rate currently supported by the LVK data.

We also acknowledge alternative formation channels, such as the inspiral of IMBHs formed via runaway collisions in dense star clusters [17], which can produce IMBH inspirals into MBHs at rates of $\sim 100 \text{ Gyr}^{-1}$ per Milky-Way-mass galaxy if IMBHs are common in globular clusters. Additionally, IMBHs may form and grow in AGN disks without necessarily merging with other black holes first. Regardless of the specific formation channel, the total mass of IMBHs captured is constrained by the global SMBH mass budget ρ_{\bullet} : the aggregate IMBH mass delivered into SMBHs cannot exceed the SMBH mass density measured today.

Finally, because IMBHs inspiral into SMBHs, the high-frequency cutoff of the background is set by the SMBH innermost stable circular orbit (ISCO) rather than a stellar-mass merger frequency. In practice, the highest frequencies are produced by captures into the *lightest* SMBHs that participate in the channel. For a Schwarzschild SMBH,

$$f_{\text{ISCO}} \simeq 4.4 \times 10^{-2} \left(\frac{10^5 M_{\odot}}{M_{\bullet}} \right) \text{ Hz}, \quad (2)$$

so an assumed minimum SMBH mass M_{\bullet}^{min} maps directly to the cutoff $f_{\text{max}} \approx f_{\text{ISCO}}(M_{\bullet}^{\text{min}})$ (up to spin factors). This dependence will enter explicitly in the background normalization below. To connect the AGN channel to the IMBH-SMBH background, we adopt a mass-budget argument in the spirit of Phinney [18], Sato-Polito *et al.* [19]. The comoving mass density processed through AGN BBH mergers is:

$$\rho_{\text{BBH}}^{\text{AGN}} \simeq f_{\text{AGN}} R_{\text{BBH}}^{\text{obs}} \langle M_{\text{BBH}} \rangle T_{\text{eff}}, \quad (3)$$

where $R_{\text{BBH}}^{\text{obs}}$ is the total BBH merger rate observed by LVK, f_{AGN} is the fraction of these mergers occurring in

TABLE I. Fiducial parameters and uncertainty ranges used to evaluate the AGN–IMRI background amplitude in Eq. (8).

Parameter	Fiducial	Range	Physical meaning
ϵ_{gw}	0.05	0.01–0.30	GW radiative efficiency (e.g., inspiral to the ISCO of a Schwarzschild SMBH; higher for prograde inspiral into spinning SMBHs).
f_{AGN}	0.1	0.01–1.0	Fraction of LVK BBH mergers occurring in AGN disks.
κ_{IM}	0.3	0.05–1.0	Efficiency of IMBH retention and eventual capture by the central SMBH.
$R_{\text{BBH}}^{\text{obs}}$	20	14–26	LVK BBH merger rate density [$\text{Gpc}^{-3} \text{yr}^{-1}$].
$\langle M_{\text{BBH}} \rangle$	60	20–150	Mean total mass of LVK BBH mergers [M_{\odot}].
T_{eff}	10	1–13	Effective cosmic integration time [Gyr].
M_{\bullet}^{min}	10^5	10^4 – 10^7	Minimum SMBH mass hosting IMBH captures [M_{\odot}] (sets f_{max}).
ρ_{\bullet}	1.8×10^6	$(1.3\text{--}2.6) \times 10^6$	Local SMBH mass density [$M_{\odot} \text{Mpc}^{-3}$], Liepold and Ma [14]

AGN disks, $\langle M_{\text{BBH}} \rangle$ is the typical merger mass, and T_{eff} is an effective cosmic integration time.

Current constraints from GWTC-4 suggest $R_{\text{BBH}}^{\text{obs}} \sim 14\text{--}26 \text{Gpc}^{-3} \text{yr}^{-1}$. We adopt a fiducial value of $20 \text{Gpc}^{-3} \text{yr}^{-1}$. The fraction f_{AGN} is uncertain but bounded by 0.01–0.3 in most models. Only a fraction of the mass processed in BBH mergers remains in IMBHs that survive, are retained in the disk, and eventually inspiral into the central SMBH. We encapsulate these efficiencies in a parameter κ_{IM} , such that the density of IMBHs accreted onto SMBHs is:

$$\rho_{\text{IMR}} = \kappa_{\text{IM}} \rho_{\text{BBH}}^{\text{AGN}}. \quad (4)$$

The fraction of the total SMBH mass assembled through this channel is then:

$$f_{\text{IMR}} = \frac{\rho_{\text{IMR}}}{\rho_{\bullet}} = \kappa_{\text{IM}} f_{\text{AGN}} \frac{R_{\text{BBH}}^{\text{obs}} \langle M_{\text{BBH}} \rangle T_{\text{eff}}}{\rho_{\bullet}}. \quad (5)$$

To determine the strength of the GWB, we utilize the energetic ceilings scaling law derived in Paper I [8]. This law relates the characteristic strain directly to the processed mass density of the source population (ρ_{src}) and the radiative efficiency (ϵ_{gw}). For the specific case of IMBHs in AGN disks, substituting $\rho_{\text{src}} = \rho_{\text{IMR}}$ yields:

$$A_{\text{IMR}} = \frac{H_0}{\pi} f_{\text{ref}}^{-2/3} f_{\text{max}}^{-1/3} \sqrt{\frac{\epsilon_{\text{gw}} \rho_{\text{IMR}}}{\rho_c}}. \quad (6)$$

$$A_{\text{IMR}} \simeq 1.2 \times 10^{-21} \left(\frac{\epsilon_{\text{gw}}}{0.05} \right)^{1/2} \left(\frac{\kappa_{\text{IM}}}{0.3} \right)^{1/2} \left(\frac{f_{\text{AGN}}}{0.1} \right)^{1/2} \left(\frac{R_{\text{BBH}}^{\text{obs}}}{20 \text{Gpc}^{-3} \text{yr}^{-1}} \right)^{1/2} \left(\frac{\langle M_{\text{BBH}} \rangle}{60 M_{\odot}} \right)^{1/2} \left(\frac{T_{\text{eff}}}{10 \text{Gyr}} \right)^{1/2} \left(\frac{M_{\bullet}^{\text{min}}}{10^5 M_{\odot}} \right)^{1/3}. \quad (8)$$

Including the uncertainty from the LVK merger rate, we obtain $A_{\text{IMR}} = (1.2_{-0.2}^{+0.2}) \times 10^{-21}$ at the reference frequency. The characteristic strain spectrum is thus:

$$h_{c,\text{IMR}}(f) \simeq 1.2 \times 10^{-21} \left(\frac{f}{3 \text{mHz}} \right)^{-2/3}. \quad (9)$$

This relation strictly bounds the background amplitude by the processed mass density ρ_{IMR} , consistent with the global conservation of energy.

IV. RESULTS

We evaluate Eq. (6) using fiducial parameters consistent with current observations (Table I). We adopt $f_{\text{ref}} = 3 \text{mHz}$ and a high-frequency cutoff $f_{\text{max}} \approx 4 \times 10^{-2} \text{Hz}$, corresponding to the ISCO of a $M_{\bullet}^{\text{min}} \sim 10^5 M_{\odot}$ SMBH (Schwarzschild; spins would shift this by factors of order unity). Based on the LVK merger rate $R_{\text{BBH}}^{\text{obs}} \approx 20 \text{Gpc}^{-3} \text{yr}^{-1}$ and an AGN fraction $f_{\text{AGN}} \approx 0.1$, the implied IMBH mass density is $\rho_{\text{IMR}} \approx 360 M_{\odot} \text{Mpc}^{-3}$. Compared to the adopted SMBH mass density $\rho_{\bullet} = (1.8_{-0.5}^{+0.8}) \times 10^6 M_{\odot} \text{Mpc}^{-3}$ [14] (Eq. 8 in Paper I), this corresponds to a capture fraction

$$f_{\text{IMR}} \equiv \frac{\rho_{\text{IMR}}}{\rho_{\bullet}} \simeq (2.0_{-0.6}^{+0.8}) \times 10^{-4}, \quad (7)$$

where the uncertainty shown is solely from propagating the asymmetric uncertainty on ρ_{\bullet} . Substituting these values into the scaling relation, we find:

This amplitude lies below the LISA confusion foreground from Galactic white dwarfs, which is typically $h_c \sim 10^{-20}$ at 3 mHz, and some EMRI GWB models [20]. However, the IMBH signal extends to higher frequencies where the WD foreground fades. The full spectral landscape

is shown in Figure 1.

The local SMBH mass density $\rho_\bullet = (1.8^{+0.8}_{-0.5}) \times 10^6 M_\odot \text{Mpc}^{-3}$ [14] has important implications for the maximum upper bound, or ceiling, of this background. The higher normalization of ρ_\bullet means that the total available mass budget for SMBH growth is larger than estimated from previous scaling relations [9, 10].

In a maximally optimistic scenario where $f_{\text{AGN}} \sim 0.3$, $\kappa_{\text{IM}} \sim 1$, and hierarchical growth is highly efficient, the IMBH capture rate could be significantly higher. However, the total mass delivered through IMBH captures cannot exceed the local SMBH mass density.

If we set $\rho_{\text{IMR}} = f_{\text{IMR}}^{\text{max}} \rho_\bullet$ with $f_{\text{IMR}}^{\text{max}} \approx 0.05$ (5% of growth from IMBHs), the amplitude rises to:

$$A_{\text{IMR}}^{\text{max}} \leq (1.9^{+0.4}_{-0.3}) \times 10^{-20}. \quad (10)$$

This represents a hard astrophysical limit. The background cannot be brighter than this without implying that IMBHs constitute the majority of SMBH mass, which is contradicted by evidence for gas accretion growth via quasars.

V. COMPARISON TO ALTERNATIVE FORMATION CHANNELS

The background derived in Eq. (6) represents the contribution from a specific sub-population: IMBHs formed or captured within AGN disks that subsequently inspiral into the central SMBH. To place this result in context, we must compare it to the primary alternative source classes discussed in the literature: dynamical cluster captures and “light” IMRIs.

A. Dynamical Cluster Infall vs. AGN Migration

The most prominent alternative formation channel for AGN–IMRI systems is the dynamical infall of dense stellar clusters (e.g., globular clusters or nuclear star clusters) due to dynamical friction. In this “dry” merger scenario, an IMBH formed in the cluster core (via runaway collisions or hierarchical mergers) is delivered to the galactic center as the host cluster dissolves [17, 24].

While both channels produce “heavy” IMRIs, they are distinguished by their orbital parameters. Dynamical captures in gas-poor environments typically enter the LISA band with high eccentricities ($e \gtrsim 0.5$) that are retained until the final stages of inspiral. In contrast, the AGN-channel inspirals modeled here are “wet” mergers: interaction with the dissipative gas disk is expected to circularize the orbit ($e \sim 0$) long before the system enters the mHz GW band [12, 16]. This circularity concentrates the signal power in the dominant $m = 2$ harmonic, distinguishing the AGN background from the spectrally richer, eccentric cluster population.

Theoretical rate estimates for the cluster channel are typically $\mathcal{R}_{\text{dyn}} \sim 0.01\text{--}0.1 \text{Gpc}^{-3}\text{yr}^{-1}$ for IMBHs in the

$10^3 M_\odot$ range [17]. It is notable that our LVK-anchored estimate yields a broadly consistent density. Our derived capture mass density $\rho_{\text{IMR}} \approx 360 M_\odot \text{Mpc}^{-3}$ implies a volumetric merger rate of:

$$\mathcal{R} \approx \frac{\rho_{\text{IMR}}}{\langle M_{\text{IMBH}} \rangle T_{\text{eff}}} \sim 0.04 \text{Gpc}^{-3}\text{yr}^{-1}, \quad (11)$$

assuming an average IMBH mass of $\sim 10^3 M_\odot$ and an effective accumulation time of 10 Gyr. This suggests that the AGN and cluster channels may contribute comparably to the “heavy” IMRI background. The total signal could thus be a superposition of circular (AGN) and eccentric (cluster) components, with the AGN component dominating the higher frequencies due to more efficient circularization.

B. Heavy vs. Light IMRIs

The terminology “IMRI” in the literature is often used to describe two physically distinct regimes. “Light” IMRIs refer to the inspiral of a stellar-mass compact object into an IMBH (e.g., $10 M_\odot + 10^3 M_\odot$) [25]. These sources probe the spacetime of the IMBH itself and are primary targets for decihertz detectors like DECIGO [26] or BBO [21], but they require a pre-existing population of wandering IMBHs in the field or in dwarf galaxies [27].

In contrast, the “heavy” IMRIs ($10^3 M_\odot + 10^6 M_\odot$) considered in this work involve the IMBH acting as the secondary. This population bridges the gap between stellar-mass EMRIs and SMBHB. By anchoring our model to the LVK merger rate [1], we translate an empirically calibrated supply of stellar-mass black holes in AGN disks into a corresponding rate of hierarchical growth, yielding a rare population of IMBH secondaries. The resulting background is therefore not dependent on an assumed primordial IMBH density, but rather on the efficiency of hierarchical growth within the disk.

C. Contrast with Forward Models

Finally, our approach differs from “forward modeling” studies that simulate specific trap efficiencies and accretion rates [4, 15, 16]. While those models delineate the parameter space allowed by disk microphysics, they often predict rates based on local conditions without explicit reference to the global SMBH mass budget. Our derivation complements these studies by providing a top-down constraint: regardless of how efficient migration traps are [28], the integrated mass flux of IMBHs cannot exceed the local SMBH mass density ρ_\bullet derived from scaling relations [14]. This energy-conservation argument provides a robust astrophysical “floor” for the background amplitude, reducing the dependence on uncertain accretion parameters.

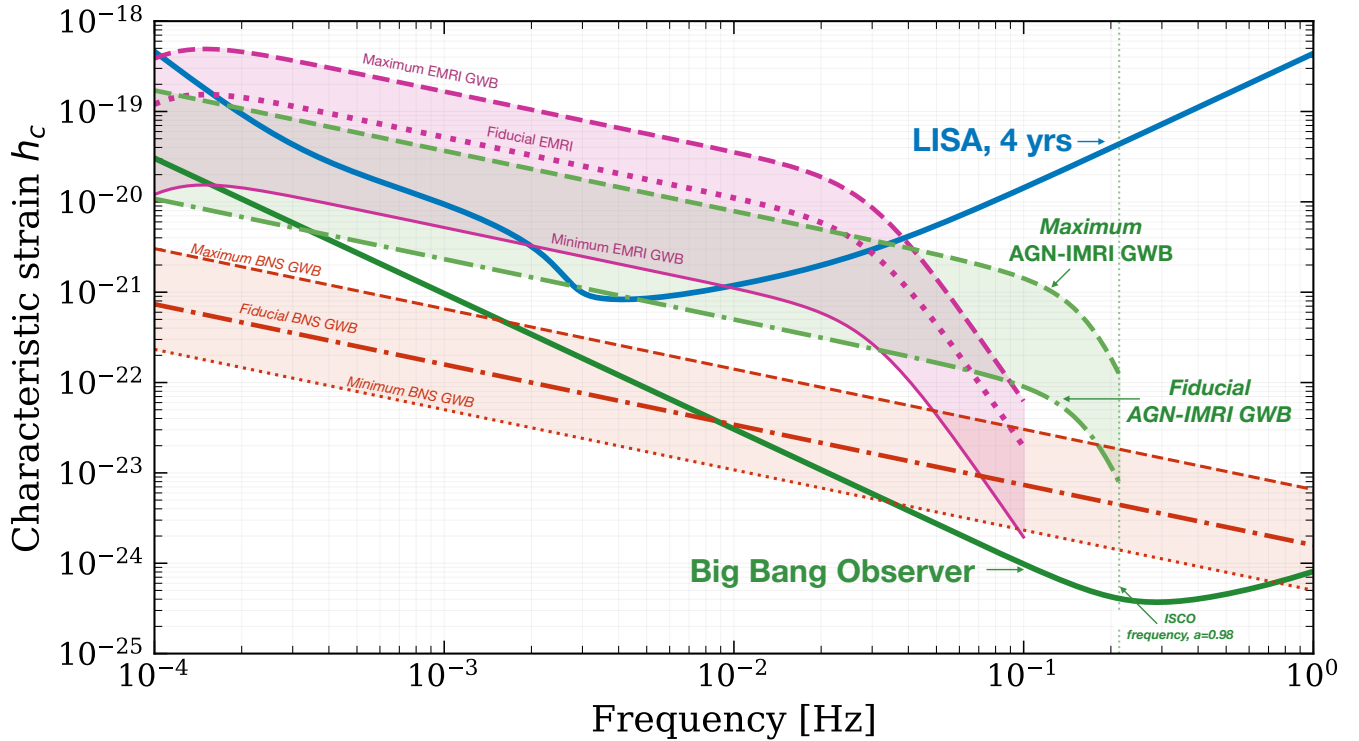


FIG. 1. Characteristic strain spectra for the AGN-IMRI background and the stellar-mass EMRI background [20], highlighting the large astrophysical uncertainties in both populations. The shaded regions bracket plausible minimum-to-maximum scenarios, with fiducial models shown as thicker curves. For the AGN-IMRI background, the high-frequency cutoff is set by the ISCO of the lightest participating SMBHs. Here we plot the AGN-IMRI GWB for a spinning, $a_\bullet = 0.98$, SMBH. A non-spinning SMBH would lower the cutoff frequency by a factor of ~ 6 . Also shown are representative strain sensitivities for a 4-year LISA mission [6] and for a Big Bang Observer (BBO)-like decihertz detector [21]. The BNS inspiral background [22, 23] is also shown, with its shaded band reflecting uncertainties in the merger rate. The fact that both the AGN-IMRI and EMRI backgrounds can rise into the 10^{-2} – 10^{-1} Hz window motivates targeted searches at higher frequencies, where the signals may become detectable even if they are subdominant near a few mHz. The Galactic white dwarf foreground appears as a bump in the LISA characteristic strain curve at around 1 mHz.

VI. COMPONENT SEPARATION

A key challenge is distinguishing the AGN-IMRI background from the Galactic DWD foreground and other extragalactic backgrounds (e.g., stellar-mass EMRIs). In what follows, we show how spectral, statistical, and modulation analyses can separate these components.

A. Separating the Galactic White Dwarf Foreground

The Galactic DWD foreground exceeds the expected IMBH background by ~ 2 orders of magnitude in the mHz band. Both signals share a nearly identical inspiral spectral slope ($h_c \propto f^{-2/3}$). However, their angular structures differ: the extragalactic background is isotropic, while the Galactic foreground is concentrated toward the Galactic plane. As LISA orbits the Sun, its antenna pattern rotates relative to the Galaxy, imposing an annual modulation on the measured Galactic power.

This modulation is absent for an isotropic background.

We decompose the cross-correlated TDI data streams into Fourier harmonics of the LISA orbital frequency $f_m = 1 \text{ yr}^{-1}$. In a narrow frequency bin centered on f , the expected signal in the k -th harmonic ($k = 0, \pm 1, \pm 2, \dots$) for channel pair IJ is:

$$\mu_k^{IJ}(f) = [A_{\text{iso}} \delta_{k0} + A_{\text{gal}} \mathcal{M}_k^{IJ}(f)] S(f), \quad (12)$$

where A_{iso} and A_{gal} are the amplitudes of the isotropic and Galactic backgrounds, $S(f)$ is the common spectral shape, and $\mathcal{M}_k^{IJ}(f)$ is the modulation transfer function encoding the LISA response to the Galactic anisotropy. The Kronecker delta δ_{k0} reflects the fact that an isotropic background produces no modulation and contributes only to $k = 0$.

The modulation coefficients \mathcal{M}_k^{IJ} depend on the Galactic geometry (primarily the $l = 2$ and $l = 4$ spherical harmonic moments of the DWD distribution) and the LISA orbit. For a disk-like distribution, power is concentrated in low-order harmonics $|k| \leq 4$ [29].

We work with log-amplitudes $\boldsymbol{\theta} = (\ln A_{\text{iso}}, \ln A_{\text{gal}})$.

The derivatives of the data model are:

$$\frac{\partial \mu_k^{IJ}}{\partial \ln A_{\text{iso}}} = A_{\text{iso}} \delta_{k0} S(f), \quad (13)$$

$$\frac{\partial \mu_k^{IJ}}{\partial \ln A_{\text{gal}}} = A_{\text{gal}} \mathcal{M}_k^{IJ} S(f). \quad (14)$$

Assuming Gaussian noise with variance $\sigma^2(f)$ per frequency bin, the Fisher information matrix is:

$$\mathcal{F}_{ab} = \sum_f \sum_{IJ} \sum_k \frac{1}{\sigma^2(f)} \frac{\partial \mu_k^{IJ}}{\partial \theta_a} \frac{\partial \mu_k^{IJ}}{\partial \theta_b}. \quad (15)$$

Evaluating the sums over k , the $k = 0$ mode contributes to all elements while $k \neq 0$ modes contribute only to \mathcal{F}_{22} :

$$\mathcal{F}_{11} = A_{\text{iso}}^2 \sum_f \frac{S^2}{\sigma^2} \sum_{IJ} 1 \equiv A_{\text{iso}}^2 W, \quad (16)$$

$$\mathcal{F}_{12} = A_{\text{iso}} A_{\text{gal}} \sum_f \frac{S^2}{\sigma^2} \sum_{IJ} \text{Re}(\mathcal{M}_0^{IJ}) \equiv A_{\text{iso}} A_{\text{gal}} W \bar{\mathcal{M}}_0, \quad (17)$$

$$\mathcal{F}_{22} = A_{\text{gal}}^2 \sum_f \frac{S^2}{\sigma^2} \sum_{IJ} \sum_k |\mathcal{M}_k^{IJ}|^2 \equiv A_{\text{gal}}^2 W \bar{\mathcal{M}}_{\text{tot}}^2, \quad (18)$$

where we have defined the total weight W , the mean DC response $\bar{\mathcal{M}}_0$, and the total modulation power $\bar{\mathcal{M}}_{\text{tot}}^2$ (all averaged over frequencies and channel pairs). We further decompose:

$$\bar{\mathcal{M}}_{\text{tot}}^2 = \bar{\mathcal{M}}_0^2 + \bar{\mathcal{M}}_{\neq 0}^2, \quad (19)$$

where $\bar{\mathcal{M}}_{\neq 0}^2 \equiv \sum_{k \neq 0} |\bar{\mathcal{M}}_k|^2$ is the power in the sidebands.

The Fisher matrix is therefore

$$\mathcal{F} = W \begin{pmatrix} A_{\text{iso}}^2 & A_{\text{iso}} A_{\text{gal}} \bar{\mathcal{M}}_0 \\ A_{\text{iso}} A_{\text{gal}} \bar{\mathcal{M}}_0 & A_{\text{gal}}^2 \bar{\mathcal{M}}_{\text{tot}}^2 \end{pmatrix}, \quad (20)$$

and the determinant is:

$$\det \mathcal{F} = W^2 A_{\text{iso}}^2 A_{\text{gal}}^2 (\bar{\mathcal{M}}_{\text{tot}}^2 - \bar{\mathcal{M}}_0^2) = W^2 A_{\text{iso}}^2 A_{\text{gal}}^2 \bar{\mathcal{M}}_{\neq 0}^2. \quad (21)$$

The marginalized variance on $\ln A_{\text{iso}}$ is the $(1, 1)$ element of the inverse:

$$\sigma_{\ln A_{\text{iso}}}^2 = (\mathcal{F}^{-1})_{11} = \frac{A_{\text{gal}}^2 \bar{\mathcal{M}}_{\text{tot}}^2}{W A_{\text{iso}}^2 A_{\text{gal}}^2 \bar{\mathcal{M}}_{\neq 0}^2} = \frac{1}{W A_{\text{iso}}^2} \frac{\bar{\mathcal{M}}_{\text{tot}}^2}{\bar{\mathcal{M}}_{\neq 0}^2}. \quad (22)$$

Taking the square root:

$$\sigma_{\ln A_{\text{iso}}} = \frac{1}{A_{\text{iso}} \sqrt{W}} \frac{\bar{\mathcal{M}}_{\text{tot}}}{\bar{\mathcal{M}}_{\neq 0}}. \quad (23)$$

This result has an important physical interpretation. The prefactor $1/(A_{\text{iso}} \sqrt{W})$ is the uncertainty one would obtain when estimating A_{iso} in isolation; it decreases with increasing signal strength and with the effective

integration weight included in W . The remaining factor, $\bar{\mathcal{M}}_{\text{tot}}/\bar{\mathcal{M}}_{\neq 0}$, quantifies the penalty incurred when marginalizing over the partially degenerate Galactic component. In the idealized limit where all Galactic power resides in the modulation sidebands (i.e., $\mathcal{M}_0 = 0$), one has $\bar{\mathcal{M}}_{\text{tot}} = \bar{\mathcal{M}}_{\neq 0}$ and the penalty is unity. In practice, $\bar{\mathcal{M}}_0 \neq 0$, so $\bar{\mathcal{M}}_{\text{tot}} > \bar{\mathcal{M}}_{\neq 0}$ and marginalization inflates the uncertainty on A_{iso} by a factor exceeding one.

If the sidebands vanish ($\bar{\mathcal{M}}_{\neq 0} \rightarrow 0$), the error diverges: $\sigma_{\ln A_{\text{iso}}} \rightarrow \infty$. This is the statement that without modulation, the two components are perfectly degenerate and cannot be separated by any analysis. The correlation coefficient between $\ln A_{\text{iso}}$ and $\ln A_{\text{gal}}$ is:

$$r = \frac{\mathcal{F}_{12}}{\sqrt{\mathcal{F}_{11} \mathcal{F}_{22}}} = \frac{\bar{\mathcal{M}}_0}{\bar{\mathcal{M}}_{\text{tot}}}. \quad (24)$$

When $\bar{\mathcal{M}}_{\neq 0} \rightarrow 0$, we have $\bar{\mathcal{M}}_{\text{tot}} \rightarrow \bar{\mathcal{M}}_0$ and $r \rightarrow 1$, which is a perfect degeneracy.

For the penalty factor to remain modest (say, $\lesssim 3$), we require $\bar{\mathcal{M}}_{\neq 0} \gtrsim \bar{\mathcal{M}}_{\text{tot}}/3$, i.e., a significant fraction of the Galactic power must reside in the sidebands. More fundamentally, the sidebands themselves must be detected above the noise. This requires:

$$\text{SNR}_{\text{mod}} \equiv \sqrt{T_{\text{obs}} \int df \sum_{IJ} \sum_{k \neq 0} \frac{|A_{\text{gal}} \mathcal{M}_k^{IJ} S(f)|^2}{P_n(f)}} \gg 1, \quad (25)$$

where $P_n(f)$ is the noise power spectral density and T_{obs} is the observation time.

For the LISA mission, the DWD foreground exceeds the instrumental noise by 1–2 orders of magnitude in the mHz band, and the Galactic disk geometry ensures $\bar{\mathcal{M}}_{\neq 0}^2/\bar{\mathcal{M}}_{\text{tot}}^2 \sim 0.1\text{--}0.3$ depending on frequency [29]. With a 4-year mission, $\text{SNR}_{\text{mod}} \sim 10^2\text{--}10^3$, easily satisfying the detectability condition. The marginalization penalty is then low given the large foreground SNR.

B. Distinguishing from Stellar-Mass EMRIs

After removing the Galactic foreground, the isotropic residual may contain both AGN-IMRI and stellar-mass EMRI signals. These can be separated by their statistical and spectral properties, which we discuss below.

The stellar-mass EMRI background originates from a large number of weak sources overlapping in the LISA band ($\mathcal{M} \sim 10 M_{\odot}$). This high duty cycle ($\mathcal{D} \gg 1$) results in a Gaussian confusion noise. In contrast, the AGN-IMRI background involves massive sources ($\mathcal{M} \sim 10^3 M_{\odot}$). To satisfy the mass budget constraint ($\rho_{\text{IMR}} < \rho_{\bullet}$), there must be far fewer of these events, leading to a low duty cycle ($\mathcal{D} \lesssim 1$). The AGN-IMRI signal will thus appear as non-Gaussian “popcorn” noise—intermittent, resolvable chirps standing out against the Gaussian EMRI floor.

Stellar-mass EMRIs are typically dynamical captures that retain high eccentricity, distributing GW power

across many harmonics and flattening the effective spectral slope. AGN-IMRIs, formed via migration in gas disks, are expected to be circularized by gas drag ($e \approx 0$). Their signal is concentrated in the $m = 2$ harmonic, strictly following the $f^{-2/3}$ inspiral power law.

VII. CONTEXT WITHIN THE STOCHASTIC GWB LANDSCAPE

This section places the AGN-IMRI background in context with the dominant stochastic signals and foregrounds expected across the mHz to decihertz band. Figure 1 provides a visual summary of the AGN-IMRI and stellar-mass EMRI ranges relative to representative detector sensitivities. The aim here is to compare which backgrounds dominate where, and to understand which qualitative features (e.g. spectral shape and annual modulation) enable separation.

At the lower end of the frequency spectrum ($f \sim 1/\text{yr}$), extrapolating the AGN-IMRI spectrum yields a characteristic strain far below the nanohertz background inferred by pulsar timing arrays. AGN-IMRI inspirals therefore cannot be a significant contributor to the PTA signal.

The most promising regime for detecting the AGN-IMRI background is the decihertz band (10^{-2} – 10^{-1} Hz), where the DWD confusion foreground rapidly diminishes while the AGN-IMRI signal rises toward its own high-frequency cutoff set by the SMBH ISCO. This is the band targeted by proposed missions such as BBO and DECIGO, and it is also where an intrinsically low duty-cycle population is least likely to be mistaken for a stationary Gaussian background.

To further contextualize the AGN-IMRI background, it is useful to compare to other extragalactic stochastic backgrounds that can overlap in frequency space. The compact-binary background from binary neutron stars (BNS) is produced by the superposition of a large number of distant inspirals [22, 23, 30, 31] and is therefore expected to be highly Gaussian, distinct from an impulsive, low-duty-cycle IMBH-driven population. Interestingly, at kHz frequencies, post-merger emission from hypermassive neutron star remnants can produce a distinct additional component of the BNS background [32, 33], which we do not explore here. The mergers of Population III remnants can also source a background whose amplitude depends sensitively on the high-redshift stellar initial mass function and binary fraction [34–36]; unlike the IMBH channel, this signal is tied directly to early-universe star formation and reionization physics.

VIII. DISCUSSION

Having established the amplitude and spectral form of the AGN-IMRI background and placed it in context with other stochastic signals and dominant foregrounds, we

now focus on interpretation and discriminants. The central question is not only whether the signal is detectable, but what a detection (or stringent upper limit) would imply for AGN-disk migration physics, hierarchical growth efficiency, and the demographics of IMBHs in galactic nuclei.

As discussed in Sec. VI B, the AGN-IMRI background is expected to manifest as non-Gaussian “popcorn” noise ($\mathcal{D} \lesssim 1$), in contrast to the Gaussian stellar-mass EMRI confusion noise ($\mathcal{D} \gg 1$). Individual IMBH events have chirp masses $\mathcal{M} \sim 10^3 M_\odot$, producing strains roughly two orders of magnitude larger than their stellar-mass counterparts ($h \propto \mathcal{M}^{5/3}$). This, combined with the global energy budget constraint of Eq. (6), implies that the AGN-IMRI background consists of intermittent, high-SNR chirps that can be individually resolved or counted using higher-order statistics (e.g., kurtosis) or matched-filter subtraction [11].

The assumption of isotropy is often applied to extragalactic backgrounds, but the finite number of sources implies a measurable level of anisotropy. Following the formalism of Mingarelli *et al.* [37], the level of anisotropy in a stochastic background scales inversely with the square root of the number of contributing sources, $\sigma_{\text{gw}}/\mu_{\text{gw}} \propto 1/\sqrt{N}$. Since the number density of AGN-IMRI systems is far lower than that of stellar-mass EMRIs, the shot noise variations in the IMBH background energy density across the sky will be significantly higher. While the stellar EMRI background will appear smooth and isotropic, the IMBH background may have a highly anisotropic spatial distribution. This spatial variance may provide an additional axis for signal separation, allowing component separation techniques to distinguish the rare, massive IMBH population from the abundant stellar population even if their frequency spectra overlap.

A detection of (or upper limit on) this background provides a direct constraint on the local number density of IMBHs in galactic nuclei. As demonstrated by Casey-Clyde *et al.* [38] in the context of pulsar timing arrays, the amplitude of a background A_{GWB}^2 is proportional to the local number density of sources, Φ_0 . By inverting this relationship, a measurement of A_{IMR} yields an estimate of $\Phi_{\text{IMR},0}$. Furthermore, this density is sensitive to the underlying physics of the black hole scaling relations. Casey-Clyde *et al.* [38] showed that assuming heavy scaling relations (e.g., Kormendy and Ho [9] or Liepold and Ma [14] relation) results in more massive black holes that evolve more rapidly due to GW emission, effectively spending less time in the detector band and lowering the observable number density compared to scaling relations that predict less massive black holes [39]. In the IMBH context, a lower-than-expected background amplitude could imply that AGN-assisted inspirals are extremely efficient (merging quickly and leaving the band) or that migration traps effectively prevent IMBHs from entering the sensitive frequency window. Thus, the background acts as a probe for the efficiency of gas-driven migration and the occupation fraction of IMBHs in AGN

disks.

Significant uncertainties remain regarding migration traps and swamps in AGN disks [40]. These structures can preferentially enhance the formation of light IMRIs (stellar BH into IMBH) relative to the heavy IMRIs (IMBH into SMBH) calculated here [28, 41]. If traps are effective, IMBHs may stall at specific radii ($100 - 1000 r_g$), potentially merging with each other rather than the central SMBH. This could suppress the mHz background derived here while enhancing the transient rate of IMBH-IMBH mergers. Conversely, if gas torques eventually drive these trapped black holes into the SMBH, the background estimate holds. The spectral shape near the cutoff f_{\max} may encode information about these final stages of migration.

Interestingly, the high-frequency cutoff of the background, determined by the ISCO of the lightest SMBHs, offers a probe of the low-mass end of the SMBH mass function. A measurement of this cutoff would constrain M_{\bullet}^{\min} and the occupation fraction of SMBHs in dwarf galaxies, a regime poorly constrained by electromagnetic observations. Furthermore, the overall amplitude is sensitive to the integrated history of gas supply in galactic nuclei. Since IMBH formation requires repeated gas-assisted mergers, the background acts as a tracer for the availability of cold gas in AGN disks over cosmic time.

IX. CONCLUSION

If AGN disks grow IMBHs that subsequently inspiral into their central SMBHs, the process must generate a

stochastic GWB whose amplitude is set by the AGN-assisted BBH rate and the cosmic SMBH mass density. We have shown that this background is bounded by the general energetic ceiling derived in Mingarelli [8]. In the simple mass-budget framework, the resulting background occupies a narrow amplitude range. We find a fiducial level $A_{\text{IMR}} \simeq 1.2 \times 10^{-21}$ at 3 mHz and a hard ceiling $A_{\text{IMR}}^{\max} \leq (1.9_{-0.3}^{+0.4}) \times 10^{-20}$ before the SMBH mass budget is saturated.

This background is a unique multi-band probe. It links the stellar-mass mergers observed by LIGO/Virgo to the supermassive black holes at galaxy centers. While challenging to detect in the LISA band due to the Galactic white dwarf foreground, it is a prime target for decihertz detectors such as BBO and DECIGO. A detection would confirm the AGN channel as a major pathway for black hole growth, while a non-detection would strictly limit the efficiency of hierarchical mergers in accretion disks.

ACKNOWLEDGMENTS

C. M. F. M. is grateful to B. Burkhart, S. E. K. Ford, B. McKernan, and V. Ozolins for useful comments. She is also grateful to E. Berti and the organizers of the “deciHz Gravitational Wave Observations on the Moon and Beyond” workshop, which motivated her to finish this work. This work was supported in part by the National Science Foundation under Grant PHY-2020265, and NASA LPS 80NSSC24K0440.

[1] The LIGO Scientific Collaboration, the Virgo Collaboration, the KAGRA Collaboration, A. G. Abac, I. Abouelfetouh, F. Acernese, K. Ackley, C. Adamcewicz, S. Adhicary, D. Adhikari, N. Adhikari, R. X. Adhikari, V. K. Adkins, S. Afroz, A. Agapito, D. Agarwal, M. Agathos, N. Aggarwal, S. Aggarwal, O. D. Aguiar, I. L. Ahrend, L. Aiello, A. Ain, P. Ajith, T. Akutsu, S. Albanesi, W. Ali, S. Al-Kershi, C. Alléné, A. Allocca, S. Al-Shammari, P. A. Altin, S. Alvarez-Lopez, W. Amar, O. Amarasinghe, A. Amato, F. Amicucci, C. Amra, A. Ananyeva, S. B. Anderson, W. G. Anderson, M. Andia, M. Ando, M. Andrés-Carcasona, T. Andrić, J. Anglin, S. Ansoldi, J. M. Antelis, S. Antier, M. Aoumi, E. Z. Appavuravther, S. Appert, S. K. Apple, K. Arai, A. Araya, M. C. Araya, M. Arca Sedda, J. S. Areeda, N. Aritomi, F. Armato, S. Armstrong, N. Arnaud, M. Arogeti, S. M. Aronson, K. G. Arun, G. Ashton, Y. Aso, L. Asprea, M. Assiduo, S. Assis de Souza Melo, S. M. Aston, P. Astone, F. Attadio, F. Aubin, K. AultONeal, G. Avallone, E. A. Avila, S. Babak, C. Badger, S. Bae, S. Bagnasco, L. Baiotti, R. Bajpai, T. Baka, A. M. Baker, K. A. Baker, T. Baker, G. Baldi, N. Baldicchi, M. Ball, G. Ballardin, S. W. Ballmer, S. Banagiri, B. Banerjee, D. Bankar, T. M. Baptiste, P. Baral, M. Baratti, J. C. Barayoga, B. C. Barish, D. Barker, N. Barman, P. Barneo, F. Barone, B. Barr, L. Barsotti, M. Barsuglia, D. Barta, A. M. Bartoletti, M. A. Barton, I. Bartos, A. Basalaev, R. Bassiri, A. Basti, M. Bawaj, P. Baxi, J. C. Bayley, A. C. Baylor, P. A. Baynard, II, M. Bazzan, V. M. Bedakihale, F. Beirnaert, M. Bejger, D. Belardinelli, A. S. Bell, D. S. Bellie, L. Bellizzi, W. Benoit, I. Bentara, J. D. Bentley, M. Ben Yaala, S. Bera, F. Bergamin, B. K. Berger, S. Bernuzzi, M. Beroiz, C. P. L. Berry, D. Bersanetti, T. Bertheas, A. Bertolini, J. Betzwieser, D. Beveridge, G. Bevilacqua, N. Bevins, R. Bhandare, R. Bhatt, D. Bhattacharjee, S. Bhattacharyya, S. Bhaumik, V. Biancalana, A. Bianchi, I. A. Bilenko, G. Billingsley, A. Binetti, S. Bini, C. Binu, S. Biot, O. Birnholtz, S. Biscoveanu, A. Bisht, M. Bitossi, M. A. Bizouard, S. Blaber, J. K. Blackburn, L. A. Blagg, C. D. Blair, D. G. Blair, N. Bode, N. Boettner, G. Boileau, M. Boldrini, G. N. Bolingbroke, A. Boliand, L. D. Bonavena, R. Bondarescu, F. Bondu, E. Bonilla, M. S. Bonilla, A. Bonino, R. Bonnand, A. Borchers, S. Borhanian, V. Boschi, S. Bose, V. Bossilkov, Y. Bothra, A. Boudon, L. Bourg, M. Boyle, A. Bozzi, C. Bradaschia, P. R. Brady, A. Branch, M. Branchesi, I. Braun, T. Briant, A. Bril-

let, M. Brinkmann, P. Brockill, and E. Brockmueller, GWTC-4.0: Updating the Gravitational-Wave Transient Catalog with Observations from the First Part of the Fourth LIGO-Virgo-KAGRA Observing Run, [arXiv e-prints](https://arxiv.org/abs/2508.18082) , [arXiv:2508.18082 \(2025\)](https://arxiv.org/abs/2508.18082), [arXiv:2508.18082 \[gr-qc\]](https://arxiv.org/abs/2508.18082).

[2] The LIGO Scientific Collaboration, the Virgo Collaboration, and the KAGRA Collaboration, Population of merging compact binaries inferred using gravitational waves through gwtc-3, *Physical Review X* **13**, 011048 (2023).

[3] R. Abbott, T. D. Abbott, S. Abraham, F. Acernese, K. Ackley, C. Adams, R. X. Adhikari, V. B. Adya, C. Affeldt, M. Agathos, K. Agatsuma, N. Aggarwal, O. D. Aguiar, A. Aich, L. Aiello, A. Ain, P. Ajith, S. Akcay, G. Allen, A. Allocca, P. A. Altin, A. Amato, S. Anand, A. Ananyeva, S. B. Anderson, W. G. Anderson, S. V. Angelova, S. Ansoldi, S. Antier, S. Appert, K. Arai, M. C. Araya, J. S. Areeda, M. Arène, N. Arnaud, S. M. Aronson, K. G. Arun, Y. Asali, S. Asenczi, G. Ashton, S. M. Aston, P. Astone, F. Aubin, P. Aufmuth, K. AultONeal, C. Austin, V. Avendano, S. Babak, P. Bacon, F. Badaracco, M. K. M. Bader, S. Bae, A. M. Baer, J. Baird, F. Baldaccini, G. Ballardin, S. W. Ballmer, A. Bals, A. Balsamo, G. Baltus, S. Banagiri, D. Bankar, R. S. Bankar, J. C. Barayoga, C. Barbieri, B. C. Barish, D. Barker, K. Barkett, P. Barneo, F. Barone, B. Barr, L. Barsotti, M. Barsuglia, D. Barta, J. Bartlett, I. Bartos, R. Bassiri, A. Basti, M. Bawaj, J. C. Bayley, M. Bazzan, B. Bécsy, M. Bejger, I. Belahcene, A. S. Bell, D. Beniwal, M. G. Benjamin, J. D. Bentley, F. Bergamin, B. K. Berger, G. Bergmann, S. Bernuzzi, C. P. L. Berry, D. Bersanetti, A. Bertolini, J. Betzwieser, R. Bhandare, A. V. Bhandari, J. Bidler, E. Biggs, I. A. Bilenko, G. Billingsley, R. Birney, O. Birnholtz, S. Biscans, M. Bischi, S. Biscoveanu, A. Bisht, G. Bissenbayeva, M. Bitossi, M. A. Bizouard, J. K. Blackburn, J. Blackman, C. D. Blair, D. G. Blair, R. M. Blair, F. Bobba, N. Bode, M. Boer, Y. Boetzel, G. Boogaert, F. Bondu, E. Bonilla, R. Bonnand, P. Booker, B. A. Boom, R. Bork, V. Boschi, S. Bose, V. Bossilkov, J. Bosveld, Y. Bouffanais, A. Bozzi, C. Bradaschia, P. R. Brady, A. Bramley, M. Branchesi, J. E. Brau, M. Breschi, T. Briant, J. H. Briggs, F. Brighenti, A. Brillet, M. Brinkmann, P. Brockill, A. F. Brooks, J. Brooks, D. D. Brown, S. Brunett, G. Bruno, R. Bruntz, A. Buikema, T. Bulik, H. J. Bulten, A. Buonanno, R. Buscicchio, D. Buskulic, R. L. Byer, M. Cabero, L. Cadonati, G. Cagnoli, C. Cahillane, J. Calderón Bustillo, J. D. Callaghan, T. A. Callister, E. Calloni, J. B. Camp, M. Canepa, K. C. Cannon, H. Cao, J. Cao, G. Carapella, F. Carbognani, S. Caride, M. F. Carney, G. Carullo, J. Casanueva Diaz, C. Casentini, J. Castañeda, S. Caudill, M. Cavaglià, F. Cavalier, R. Cavalieri, G. Celli, P. Cerdá-Durán, E. Cesarini, O. Chaibi, K. Chakravarti, C. Chan, M. Chan, K. Chandra, S. Chao, P. Charlton, E. A. Chase, E. Chassande-Mottin, D. Chatterjee, M. Chaturvedi, K. Chatzioannou, H. Y. Chen, and X. Chen, GW190521: A Binary Black Hole Merger with a Total Mass of $150 M_\odot$, *Phys. Rev. Lett.* **125**, 101102 (2020), [arXiv:2009.01075 \[gr-qc\]](https://arxiv.org/abs/2009.01075).

[4] K. E. S. Ford and B. McKernan, Using gravitational waves and multi-messenger Astronomy to reverse-engineer the properties of galactic nuclei, [arXiv e-prints](https://arxiv.org/abs/2506.08801) , [arXiv:2506.08801 \(2025\)](https://arxiv.org/abs/2506.08801), [arXiv:2506.08801 \[astro-ph.HE\]](https://arxiv.org/abs/2506.08801).

[5] A. Sesana and D. G. Figueroa, Nanohertz Gravitational Waves, [arXiv e-prints](https://arxiv.org/abs/2512.18822) , [arXiv:2512.18822 \(2025\)](https://arxiv.org/abs/2512.18822), [arXiv:2512.18822 \[astro-ph.CO\]](https://arxiv.org/abs/2512.18822).

[6] P. Amaro-Seoane, H. Audley, S. Babak, J. Baker, E. Bausse, P. Bender, E. Berti, P. Binetruy, M. Born, D. Bortoluzzi, J. Camp, C. Caprini, V. Cardoso, M. Colpi, J. Conklin, N. Cornish, C. Cutler, K. Danzmann, R. Dolesi, L. Ferraioli, V. Ferroni, E. Fitzsimons, J. Gair, L. Gesa Bote, D. Giardini, F. Gibert, C. Grimani, H. Halloin, G. Heinzel, T. Hertog, M. Hewitson, K. Holley-Bockelmann, D. Hollington, M. Hueller, H. Inchauspe, P. Jetzer, N. Karnesis, C. Killow, A. Klein, B. Klipstein, N. Korsakova, S. L. Larson, J. Livas, I. Lloro, N. Man, D. Mance, J. Martino, I. Mateos, K. McKenzie, S. T. McWilliams, C. Miller, G. Mueller, G. Nardini, G. Nelemans, M. Nofrarias, A. Petiteau, P. Pivato, E. Plagnol, E. Porter, J. Reiche, D. Robertson, N. Robertson, E. Rossi, G. Russano, B. Schutz, A. Sesana, D. Shoemaker, J. Slutsky, C. F. Sopuerta, T. Sumner, N. Tamani, I. Thorpe, M. Troebs, M. Valisneri, A. Vecchio, D. Vetrugno, S. Vitale, M. Volonteri, G. Wanner, H. Ward, P. Wass, W. Weber, J. Ziemer, and P. Zweifel, Laser Interferometer Space Antenna, [arXiv e-prints](https://arxiv.org/abs/1702.00786) , [arXiv:1702.00786 \(2017\)](https://arxiv.org/abs/1702.00786), [arXiv:1702.00786 \[astro-ph.IM\]](https://arxiv.org/abs/1702.00786).

[7] D. Reitze, R. X. Adhikari, S. Ballmer, B. Barish, L. Barsotti, G. Billingsley, D. A. Brown, Y. Chen, D. Coyne, R. Eisenstein, M. Evans, P. Fritschel, E. D. Hall, A. Lazarini, G. Lovelace, J. Read, B. S. Sathyaprakash, D. Shoemaker, J. Smith, C. Torrie, S. Vitale, R. Weiss, C. Wipf, and M. Zucker, Cosmic Explorer: The U.S. Contribution to Gravitational-Wave Astronomy beyond LIGO, in *Bulletin of the American Astronomical Society*, Vol. 51 (2019) p. 35, [arXiv:1907.04833 \[astro-ph.IM\]](https://arxiv.org/abs/1907.04833).

[8] C. M. F. Mingarelli, Energetic Ceilings of Astrophysical Gravitational-Wave Backgrounds, [arXiv e-prints](https://arxiv.org/abs/2601.18859) , [arXiv:2601.18859 \(2026\)](https://arxiv.org/abs/2601.18859), [arXiv:2601.18859 \[astro-ph.HE\]](https://arxiv.org/abs/2601.18859).

[9] J. Kormendy and L. C. Ho, Coevolution (Or Not) of Supermassive Black Holes and Host Galaxies, *ARA&A* **51**, 511 (2013), [arXiv:1304.7762 \[astro-ph.CO\]](https://arxiv.org/abs/1304.7762).

[10] N. J. McConnell and C.-P. Ma, Revisiting the Scaling Relations of Black Hole Masses and Host Galaxy Properties, *Astrophys. J.* **764**, 184 (2013), [arXiv:1211.2816 \[astro-ph.CO\]](https://arxiv.org/abs/1211.2816).

[11] N. Cornish and T. Robson, Galactic binary science with the new LISA design, *Journal of Physics: Conference Series* **840**, 012024 (2017), [arXiv:1703.09858](https://arxiv.org/abs/1703.09858).

[12] B. McKernan, K. E. S. Ford, W. Lyra, and H. B. Perets, Intermediate mass black holes in AGN discs - I. Production and growth, *MNRAS* **425**, 460 (2012), [arXiv:1206.2309 \[astro-ph.GA\]](https://arxiv.org/abs/1206.2309).

[13] N. C. Stone and B. D. Metzger, Rates of stellar tidal disruption as probes of the supermassive black hole mass function, *MNRAS* **455**, 859 (2016), [arXiv:1410.7772 \[astro-ph.HE\]](https://arxiv.org/abs/1410.7772).

[14] E. R. Liepold and C.-P. Ma, Big Galaxies and Big Black Holes: The Massive Ends of the Local Stellar and Black Hole Mass Functions and the Implications for Nanohertz Gravitational Waves, *ApJL* **971**, L29 (2024), [arXiv:2407.14595 \[astro-ph.GA\]](https://arxiv.org/abs/2407.14595).

[15] N. W. C. Leigh, A. M. Geller, B. McKernan, K. E. S.

Ford, M.-M. Mac Low, J. Bellovary, Z. Haiman, W. Lyra, J. Samsing, M. O'Dowd, B. Kocsis, and S. Endlich, On the rate of black hole binary mergers in galactic nuclei due to dynamical hardening, *MNRAS* **474**, 5672 (2018), arXiv:1711.10494 [astro-ph.GA].

[16] H. Tagawa, Z. Haiman, and B. Kocsis, Formation and Evolution of Compact-object Binaries in AGN Disks, *Astrophys. J.* **898**, 25 (2020), arXiv:1912.08218 [astro-ph.GA].

[17] S. F. Portegies Zwart, H. Baumgardt, P. Hut, J. Makino, and S. L. W. McMillan, Formation of massive black holes through runaway collisions in dense star clusters, *Nature* **428**, 724 (2004).

[18] E. S. Phinney, A Practical Theorem on Gravitational Wave Backgrounds, *arXiv e-prints*, astro-ph/0108028 (2001), arXiv:astro-ph/0108028 [astro-ph].

[19] G. Sato-Polito, M. Zaldarriaga, and E. Quataert, Where are the supermassive black holes measured by PTAs?, *Phys. Rev. D* **110**, 063020 (2024).

[20] M. Bonetti and A. Sesana, Gravitational wave background from extreme mass ratio inspirals, *Phys. Rev. D* **102**, 103023 (2020), arXiv:2007.14403.

[21] G. M. Harry, P. Fritschel, D. A. Shaddock, W. Folkner, and E. S. Phinney, Laser interferometry for the Big Bang Observer, *Classical and Quantum Gravity* **23**, 4887 (2006).

[22] B. P. Abbott *et al.* (LIGO Scientific, Virgo), GW170817: Implications for the Stochastic Gravitational-Wave Background from Compact Binary Coalescences, *Phys. Rev. Lett.* **120**, 091101 (2018), arXiv:1710.05837 [gr-qc].

[23] M. Ebersold and T. Regimbau, Uncertainty in predicting the stochastic gravitational wave background from compact binary coalescences, (2025), arXiv:2510.02163, arXiv:2510.02163 [gr-qc].

[24] G. Ogiya, O. Hahn, C. M. F. Mingarelli, and M. Volonteri, Accelerated orbital decay of supermassive black hole binaries in merging nuclear star clusters, *MNRAS* **493**, 3676 (2020), arXiv:1911.11526 [astro-ph.GA].

[25] J. R. Gair, L. Barack, T. Creighton, C. Cutler, S. L. Larson, E. S. Phinney, and M. Vallisneri, Event rate estimates for LISA extreme mass ratio capture sources, *Classical and Quantum Gravity* **21**, S1595 (2004), arXiv:gr-qc/0405137 [gr-qc].

[26] S. Kawamura *et al.*, Current status of space gravitational wave antenna DECIGO and B-DECIGO, *Progress of Theoretical and Experimental Physics* **2021**, 05A105 (2021), arXiv:2006.13545 [gr-qc].

[27] J. E. Greene, J. Strader, and L. C. Ho, Intermediate-Mass Black Holes, *ARA&A* **58**, 257 (2020), arXiv:1911.09678 [astro-ph.GA].

[28] J. M. Bellovary, M.-M. Mac Low, B. McKernan, and K. E. S. Ford, Migration Traps in Disks around Supermassive Black Holes, *ApJL* **819**, L17 (2016), arXiv:1511.00005 [astro-ph.GA].

[29] K. Breivik, C. M. F. Mingarelli, and S. L. Larson, Constraining Galactic Structure with the LISA White Dwarf Foreground, *Astrophys. J.* **901**, 4 (2020), arXiv:1912.02200 [astro-ph.GA].

[30] T. Regimbau, The astrophysical gravitational wave stochastic background, *Research in Astronomy and Astrophysics* **11**, 369 (2011), arXiv:1101.2762 [astro-ph.CO].

[31] X.-J. Zhu, E. Howell, T. Regimbau, D. Blair, and Z.-H. Zhu, Stochastic Gravitational Wave Background from Coalescing Binary Black Holes, *Astrophys. J.* **739**, 86 (2011), arXiv:1104.3565 [gr-qc].

[32] K. Takami, L. Rezzolla, and L. Baiotti, Spectral properties of the post-merger gravitational-wave signal from binary neutron stars, *Phys. Rev. D* **91**, 064001 (2015), arXiv:1412.3240 [gr-qc].

[33] L. Lehoczky, I. Dvorkin, and L. Rezzolla, Postmerger: a new and dominant contribution to the gravitational-wave background from binary neutron stars, (2025), arXiv:2503.20877, arXiv:2503.20877 [astro-ph.HE].

[34] K. Inayoshi, K. Kashiyama, E. Visbal, and Z. Haiman, Gravitational wave background from Population III binary black holes consistent with cosmic reionization, *Mon. Not. Roy. Astron. Soc.* **461**, 2722 (2016), arXiv:1603.06921 [astro-ph.GA].

[35] T. Kinugawa, K. Inayoshi, K. Hotokezaka, D. Nakauchi, and T. Nakamura, Possible indirect confirmation of the existence of Pop III massive stars by gravitational wave, *MNRAS* **442**, 2963 (2014), arXiv:1402.6672 [astro-ph.HE].

[36] K. Inayoshi, E. Visbal, and Z. Haiman, The Assembly of the First Massive Black Holes, *ARA&A* **58**, 27 (2020), arXiv:1911.05791 [astro-ph.GA].

[37] C. M. F. Mingarelli, T. Sidery, I. Mandel, and A. Vecchio, Characterizing gravitational wave stochastic background anisotropy with pulsar timing arrays, *Phys. Rev. D* **88**, 062005 (2013), arXiv:1306.5394 [astro-ph.HE].

[38] J. A. Casey-Clyde, C. M. F. Mingarelli, J. E. Greene, K. Pardo, M. Nañez, and A. D. Goulding, A Quasar-based Supermassive Black Hole Binary Population Model: Implications for the Gravitational Wave Background, *Astrophys. J.* **924**, 93 (2022), arXiv:2107.11390 [astro-ph.HE].

[39] T. T. Ananna, C. M. Urry, E. Treister, R. C. Hickox, F. Shankar, C. Ricci, N. Cappelluti, S. Marchesi, and T. J. Turner, Accretion History of AGNs. III. Radiative Efficiency and AGN Contribution to Reionization, *Astrophys. J.* **903**, 85 (2020), arXiv:2009.07711 [astro-ph.HE].

[40] M. Cantiello, A. S. Jermyn, and D. N. C. Lin, Stellar evolution in agn disks, *Astrophys. J.* **910**, 94 (2021).

[41] E. Grishin, S. Gilbaum, and N. C. Stone, The effect of thermal torques on AGN disc migration traps and gravitational wave populations, *MNRAS* **530**, 2114 (2024), arXiv:2307.07546 [astro-ph.HE].